Direct torque control for dual three-phase induction motor drives

Direct Torque Control for Dual Three-Phase Induction Motor Drives

Radu Bojoi, Francesco Farina, Giovanni Griva, Francesco Profumo, *Senior Member, IEEE*, and Alberto Tenconi, *Member, IEEE*

***Abstract*—A direct torque control (DTC) strategy for dual three-phase induction motor drives is discussed in this paper. The induction machine has two sets of stator three-phase windings spatially shifted by 30 electrical degrees. The DTC strategy is based on a predictive algorithm and is implemented in a synchronous reference frame aligned with the machine stator flux vector. The advantages of the discussed control strategy are constant inverter switching frequency, good transient and steady-state performance, and low distortion of machine currents with respect to direct self-control (DSC) and other DTC schemes with variable switching frequency. Experimental results are presented for a 10-kW DTC dual three-phase induction motor drive prototype.**

***Index Terms*—Deadbeat algorithm, digital control, direct torque control, dual three-phase induction machine, multiphase drives.**

I. Introduction

THE MAIN advantage of multiphase drives is the possibility to divide the controlled power on more inverter legs. That will reduce the current stress of each switch compared with a three-phase converter. For this reason, multiphase drives are convenient in high-power and/or high-current applications such as ship propulsion, aerospace applications, and electric/hybrid vehicles. Other potential advantages of multiphase drives over three-phase ones are [1]–[4]: 1) lower torque pulsations at high frequency; 2) reduced rotor harmonic currents for induction motor drives; 3) higher power per rms ampere ratio for the same machine volume; and 4) reduced harmonic content of the dc-link current in case of voltage source inverter (VSI)-fed drives. Other potential advantages concern a higher reliability at system level, since a multiphase induction machine can operate with an asymmetric winding structure in case of loss of one or more inverter legs/machine phases.

A very interesting and discussed in the literature multiphase solution is the dual three-phase induction machine having two sets of three-phase windings spatially shifted by 30 electrical degrees with isolated neutral points (Fig. 1).

In applications like electrical vehicles, often the low available dc-link voltage imposes high phase currents for a three-phase drive. In this case, the dual three-phase induction machine could be an interesting alternative to the conventional three-phase counterpart. In addition, the redundancy of the phase number can be exploited in case of failures [4].

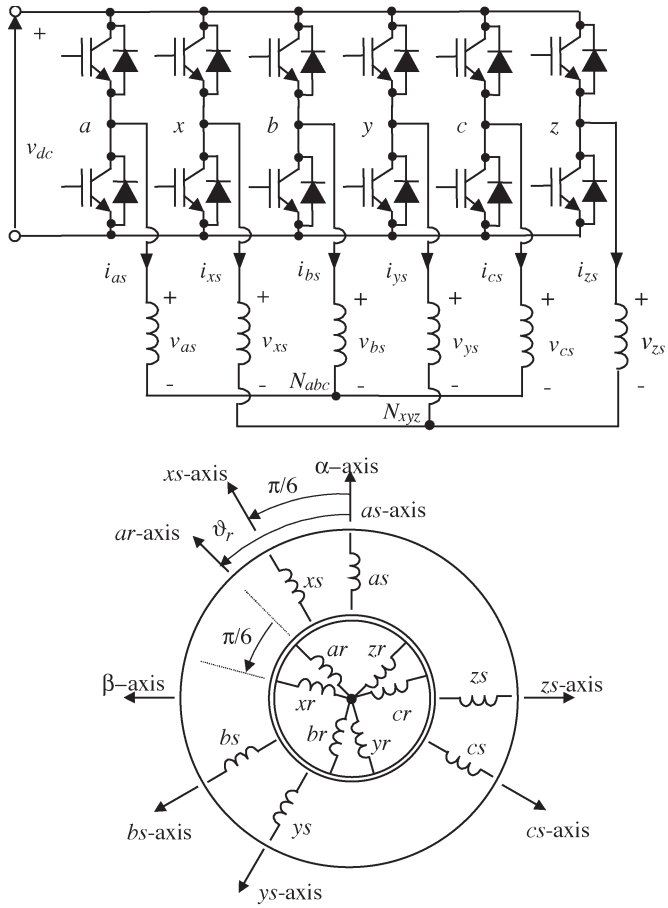

Fig. 1. Dual three-phase induction machine.

During the last three decades, the literature related to dual three-phase induction motor drives has covered an entire path: from machine modeling and design [5]–[8], through the steady-state analysis of the six-step operation using voltage source or current source inverters [9], [10], to vector control [11] using suitable pulsewidth-modulation (PWM) techniques [12]–[14] and current control solutions [15].

Traction drives require accurate control of machine flux and torque. The volt per hertz control solutions for dual three-phase induction motor drives [9] have limited performance. For this reason, a rotor field-oriented control (RFOC) solution has been proposed in [11] in order to get decoupled control of the flux and torque. The RFOC scheme must use current control

Paper IPCSD-05-057, presented at the 2004 Industry Applications Society Annual Meeting, Seattle, WA, October 3–7, and approved for publication in the IEEE TRANSACTIONS ON INDUSTRY APPLICATIONS by the Industrial Drives Committee of the IEEE Industry Applications Society. Manuscript submitted for review January 14, 2005 and released for publication September 1, 2005.

The authors are with the Dipartimento di Ingegneria Elettrica Industriale Politecnico di Torino, 10129 Turin, Italy (e-mail: radu.bojoi@polito.it; francesco.farina@polito.it; giovanni.griva@polito.it; francesco.profumo@polito.it; alberto.tenconi@polito.it).

Digital Object Identifier 10.1109/TIA.2005.858281

loops to impose the flux and torque, producing stator current components. An alternative solution is the use of direct torque control (DTC) strategies [16], [17]. In the literature, there are only a few references concerning DTC multiphase induction motor drives; such references are related mainly to five-phase induction motors [18].

To simplify the control scheme and to improve the dynamic performance by eliminating the current control loops, the proposed paper presents a DTC solution for dual three-phase induction motor drives as a possible alternative to FOC schemes.

II. Machine Model

To model the dual three-phase induction machine, the vector space decomposition (VSD) approach [12] has been used under the following assumptions.

- The windings are sinusoidally distributed and the rotor cage is equivalent to a six-phase wound rotor.
- The magnetic saturation and the core losses are neglected. The mutual leakage inductances are zero since the machine uses full-pitch stator windings.

According to the VSD, the original six-dimensional (6-D) system of the machine can be decomposed into three orthogonal subspaces (α,β), (μ_1,μ_2), and (z_1,z_2), introducing a 6×6 transformation matrix $[T_6]$ [12] having the following properties.

- The fundamental components of the machine variables and the harmonics of order $k=12n\pm 1,(n=1,2,3,\ldots)$ are mapped in the (α,β) subspace. These components contribute to the air-gap flux.
- The harmonics of order $k=6n\pm 1,(n=1,3,5,\ldots)$ are transformed in the (μ_1,μ_2) subspace. These harmonics (the 5th, 7th, 17th, 19th, ...) do not contribute to the air-gap flux since the (α,β) and (μ_1,μ_2) subspaces are orthogonal.
- The zero-sequence components are mapped in the (z_1,z_2) subspace.

Hence, from the point of view of flux and torque production, the analysis and control of the machine using the VSD approach are greatly simplified since the machine model in the (α,β) subspace is identical to the model of a three-phase machine (Fig. 2).

If the two stator sets have isolated neutral points (Fig. 1), it can be demonstrated that no current components flow in the (z_1,z_2) subspace [12]. For this reason, the machine model referred to the stationary reference frame can be reduced to two sets of decoupled equations corresponding to the machine (α,β) and (μ_1,μ_2) subspaces [11].

A. Machine Model in the (α,β) Subspace

$$\begin{cases} \overline{v}_s = R_s\bar{i}_s + p\overline{\lambda}_s \\ 0 = R_r\bar{i}_r + p\overline{\lambda}_r - j\omega_r\overline{\lambda}_r \\ \overline{\lambda}_s = L_s\bar{i}_s + M\bar{i}_r \\ \overline{\lambda}_r = M\bar{i}_s + L_r\bar{i}_r \\ T_e = 3\frac{P}{2}(\lambda_{s\alpha}i_{s\beta} - \lambda_{s\beta}i_{s\alpha}) \end{cases} \quad \begin{cases} \overline{v}_s = v_{s\alpha} + jv_{s\beta} \\ \bar{i}_s = i_{s\alpha} + ji_{s\beta} \\ \bar{i}_r = i_{r\alpha} + ji_{r\beta} \\ \overline{\lambda}_s = \lambda_{s\alpha} + j\lambda_{s\beta} \\ \overline{\lambda}_r = \lambda_{r\alpha} + j\lambda_{r\beta} \end{cases} \tag{1}$$

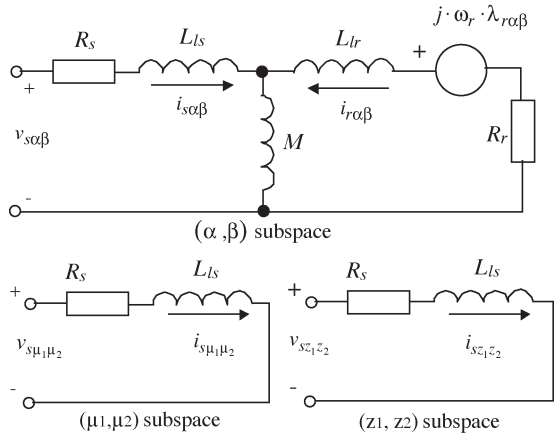

Fig. 2. Single-phase equivalent circuits of the machine.

where ω_r is the rotor speed, P is the number of poles, and $p=d/dt$. The machine parameters are reported in the Appendix.

As shown in (1), flux and torque production involves only quantities in the (α,β) subspace, and consequently machine control is simplified since it needs to act only on a two-dimensional (2-D) subspace. Thus, machine flux and torque are controlled with the voltage commands in (α,β) subspace, so flux estimation can use estimators normally employed for three-phase machines.

B. Machine Model in the (μ_1,μ_2) Subspace

$$\begin{bmatrix} v_{s\mu_1} \\ v_{s\mu_2} \end{bmatrix} = \begin{bmatrix} R_s + L_{ls}p & 0 \\ 0 & R_s + L_{ls}p \end{bmatrix} \begin{bmatrix} i_{s\mu_1} \\ i_{s\mu_2} \end{bmatrix}. \tag{2}$$

The specific aspect of dual three-phase machines is that the PWM modulation technique must simultaneously obtain the voltage commands in the (α,β) subspace and minimize the harmonic voltages generated in the (μ_1,μ_2) subspace [12]–[14]. These harmonic voltages must be as low as possible to avoid large stator loss-producing current harmonics of order $k=6n\pm 1$ [12], [13].

III. DTC Control Scheme

The main goal of a DTC scheme is to obtain a fast decoupled control of the stator flux and the electromagnetic torque without inner current control loops [16]. From the literature, the more interesting DTC solutions can be divided into two main groups:

- direct self-control (DSC) and switching table-based DTC (ST-DTC); these solutions give variable switching frequency;
- DTC based on the deadbeat solution of the machine equations; this strategy imposes constant switching frequency and also requires a PWM.

A. DSC and DTC Based on Switching Table

As shown in [12], a six-phase inverter provides 48 independent nonzero vectors and one zero vector to form a 12-sided four-layer polygon in each machine subspace. Even with

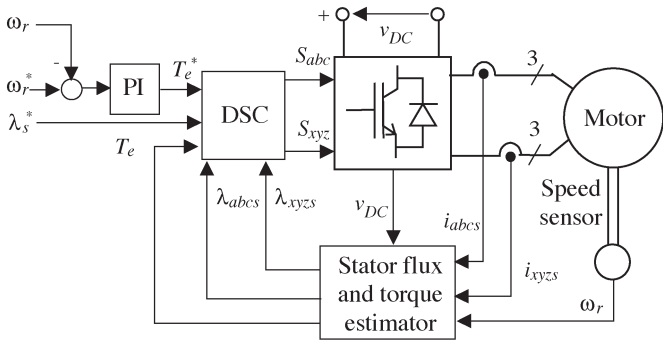

Fig. 3. Simulated DSC scheme for dual three-phase induction motor drive.

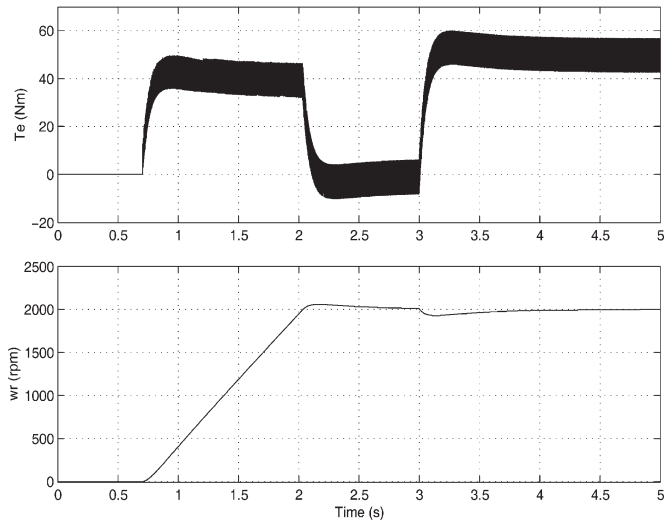

Fig. 4. Simulation results for the DSC strategy showing the machine startup. (Top) T_e (Nm). (Bottom) ω_r (r/min).

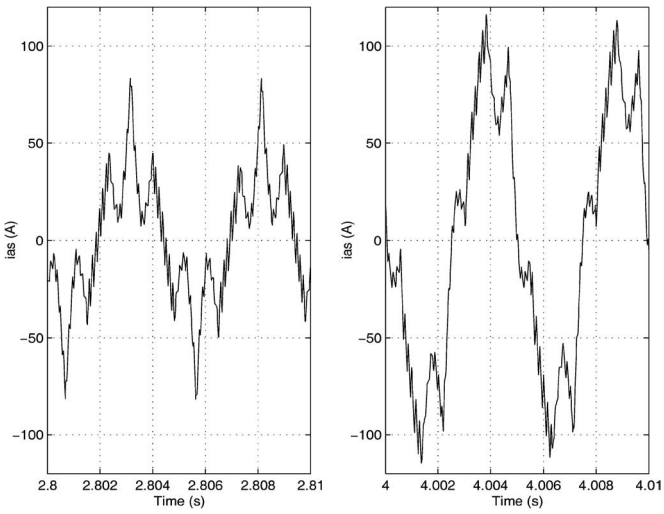

Fig. 5. Simulation results for the DSC strategy. (Left) i_{as} (A) at no load. (Right) i_{as} (A) at rated load.

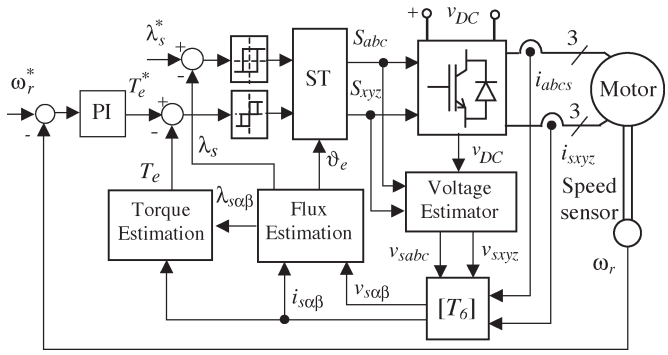

Fig. 6. Simulated ST-DTC scheme for a dual three-phase induction motor drive.

a larger number of available voltage vectors compared with the case of three-phase inverters, the DSC [19] and the ST-DTC [16] are seriously penalized by the relatively high harmonic content of the phase currents due to the current harmonics generated in the (μ_1, μ_2) subspace. Thus, the overall drive efficiency will be reduced. As an example, a DSC scheme has been simulated for the dual three-phase induction machine prototype considered in this paper using the schematic block diagram in Fig. 3. The hysteresis band for the torque controller has been set at 10% rated torque. The simulation results are shown in Figs. 4 and 5 for the drive startup at no load followed by a rated load step change.

The simulation results for the DSC show distorted phase currents, especially at light load. For this reason, this strategy is suitable only for high-power low switching frequency applications such as traction drives [19], [20].

An ST-DTC basic scheme, implemented as for three-phase machines [16], [17], has been simulated using the schematic block illustrated in Fig. 6 under the same operating conditions as the DSC scheme.

Based on the estimated stator flux position, torque (three-level) and flux (two-level) hysteresis regulators are used to generate the inverter switching functions by means of a switching table (Fig. 6). The ST-DTC strategy is based on the VSD approach and uses only voltage vectors from the external layer of a 12-sided polygon in the (α, β) subspace [12], [13] together with the zero vector. This technique is the extension of that used for three-phase drives [16], [17], where six nonzero voltage vectors (forming a six-side polygon) and a zero vector are used.

The simulation results for the ST-DTC scheme (Figs. 7 and 8) are similar with those obtained for the DSC in terms of phase current distortion since only the (α, β) subspace is controlled. However, some improvements for the ST-DTC scheme can be obtained for dual three-phase machines. The key issue is the ST design and the DTC strategy in order to get sinusoidal machine phase currents by minimizing the current components in the (μ_1, μ_2) subspace. Different ST design solutions and ST-DTC techniques have been discussed and experimented in [21] with good torque and flux regulation performance but without solving completely the phase currents distortion problem. For this reason, the ST-DTC for dual three-phase drives can be considered as an interesting topic subjected to further improvements, and more research work is expected to be performed in the future.

B. Deadbeat DTC

In some applications, it is preferred to have constant switching frequency to obtain quasi-sinusoidal phase currents. In

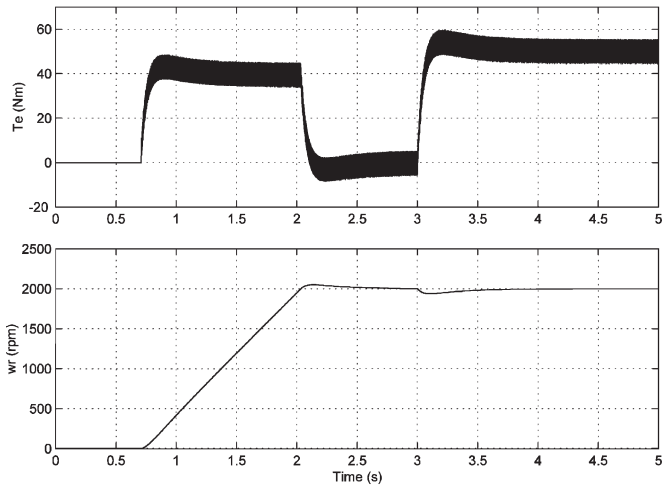

Fig. 7. Simulation results for the ST-DTC strategy showing the machine startup. (Top) T_e (Nm). (Bottom) ω_r (r/min).

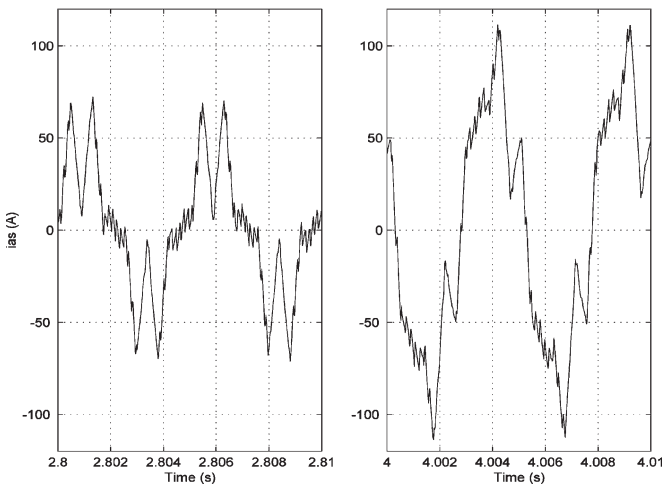

Fig. 8. Simulation results for the ST-DTC strategy. (Left) i_{as} (A) at no load. (Right) i_{as} (A) at rated load.

this case, the mean values of torque and flux are controlled over a constant sampling period. A digital direct mean torque control (DMTC) technique has been presented in [22] for three-phase induction motor drives, where a prediction of the inverter switching instants is performed in order to yield constant inverter switching frequency.

The deadbeat DTC scheme presented in this paper aims at computing an average stator voltage command vector in order to control the mean values of the stator flux and the electromagnetic torque over a sampling period. This technique uses PWM inverter operation with constant switching frequency; quasi-sinusoidal phase currents are obtained using appropriate PWM strategies [12]–[14].

The DTC scheme used in this paper is based on the simplified circuit shown in Fig. 9, where R_s is the stator resistance, L'_s is the stator transient inductance, and $\overline{e}_s$ is the back electromotive force (EMF) to be estimated from the machine model.

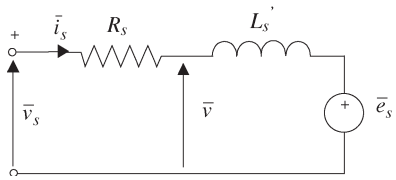

Fig. 9. Simplified equivalent circuit of the machine model in (α, β) using the VSD approach.

The mathematical background of the DTC scheme is based on that described in [23] and [24]. The time derivative of the machine torque obtained from (1) is

$$\frac{dT_e}{dt} = 3\frac{P}{2}\left(\frac{d\overline{\lambda}_s}{dt}\bar{i}_s + \overline{\lambda}_s\frac{d\bar{i}_s}{dt}\right). \tag{3}$$

The discretized form of (3), using a first-order approximation, is

$$\frac{T_e(k+1)-T_e(k)}{T_s} = 3\frac{P}{2}\left(\frac{\overline{\lambda}_s(k+1)-\overline{\lambda}_s(k)}{T_s}\bar{i}_s(k) + \overline{\lambda}_s(k)\frac{\bar{i}_s(k+1)-\bar{i}_s(k)}{T_s}\right) \tag{4}$$

where T_s is the sampling time of the DTC algorithm.

The DTC deadbeat approach aims at obtaining the reference values of the electromagnetic torque T_e^* and stator flux λ_s^* in just one sampling time, i.e.,

$$\begin{cases} T_e^* = T_e(k+1) \\ \overline{\lambda}_s^* = \overline{\lambda}_s(k+1). \end{cases} \tag{5}$$

In this case, (4) becomes

$$\Delta T_e = \frac{3}{2}P(\Delta\overline{\lambda}_s\bar{i}_s + \overline{\lambda}_s\Delta\bar{i}_s) \tag{6}$$

where $\Delta T_e = T_e^* - T_e$ is the torque variation to be produced by the variations of the stator flux $\Delta\overline{\lambda}_s = \overline{\lambda}_s^* - \overline{\lambda}_s$ and the stator current $\Delta\bar{i}_s$ vectors over one sampling time T_s. The torque value T_e and also the stator flux vector $\overline{\lambda}_s$ are estimated quantities at the current (kth) sampling time.

Due to the large field-weakening range imposed to the drive, the stator flux variation $\Delta\overline{\lambda}_s$ has been taken into account, while in [23] and [24] it has been neglected. Based on the equivalent circuit of Fig. 9, (6) becomes

$$\frac{2\Delta T_e L'_s}{3PT_s} = \overline{v}^*\left(L'_s\bar{i}_s\right) + \overline{\lambda}_s\left(\overline{v}_s^* - \overline{e}_s\right) \tag{7}$$

where $\overline{v}^*$ is the voltage vector that will achieve the deadbeat control of the torque. After adding to $\overline{v}^*$ the voltage drop across the stator resistance, the stator voltage command vector $\overline{v}_s^*$ will be obtained.

To simplify the computational effort, the deadbeat algorithm has been implemented in a (d, q) synchronous reference frame

aligned with the stator flux vector. In this case, only the command voltage on the d-axis behind the stator resistance will impose the stator flux variation, i.e.,

$$v_d^* = \frac{\Delta\overline{\lambda}_s}{T_s} = \frac{\lambda_s^* - \lambda_s}{T_s}. \tag{8}$$

The q-axis reference voltage that will achieve the deadbeat control of the torque can be easily obtained from (7) as

$$v_q^* = \frac{\frac{2\Delta T_e L_s'}{3PT_s} - v_d^* L_s' i_{qs} + \lambda_s e_{qs}}{\lambda_s - L_s' i_{ds}}. \tag{9}$$

Besides the advantages regarding the simplicity of the algorithm, the implementation in synchronous reference frame avoids the problems related to the division by zero, which occurs for stationary frame implementation [23]. Thus, the additional rotational transformations required by the (d,q) implementation are justified. Furthermore, they do not represent an important computational effort for the digital processor.

The back-EMF component e_{qs} in the synchronous reference frame can be computed by applying the rotational transformation $(\alpha,\beta) \rightarrow (d,q)$ to the back-EMF components computed in the (α,β) stationary reference frame. These voltages are computed from (1) as

$$\begin{cases} e_{s\alpha} = -\frac{1}{\tau_r}\left(\lambda_{s\alpha} - L_s i_{s\alpha}\right) - \omega_r\left(\lambda_{s\beta} - L_s' i_{s\beta}\right) \\ e_{s\beta} = -\frac{1}{\tau_r}\left(\lambda_{s\beta} - L_s i_{s\beta}\right) + \omega_r\left(\lambda_{s\alpha} - L_s' i_{s\alpha}\right) \end{cases} \tag{10}$$

where $\tau_r = L_r/R_r$ is the rotor time constant, and $\lambda_{s\alpha}$ and $\lambda_{s\beta}$ are the stator flux components in stationary frame that are estimated by a stator flux estimator.

Once the reference vector $\overline{v}^{e*}$ is computed in (d,q) synchronous reference frame, the stator reference voltage vector $\overline{v}_s^*$ in the (α,β) stationary reference frame is obtained performing an inverse rotational transformation and subsequently adding the voltage drop across the stator resistance, i.e.,

$$\overline{v}_s^* = \overline{v}^{e*} e^{j\vartheta_e} + R_s \overline{i}_s \tag{11}$$

where ϑ_e is the stator flux vector position provided by a stator flux estimator.

Based on (7)–(11), the presented algorithm is able to simultaneously control both the stator flux and the machine torque in a deadbeat fashion with high dynamic performance without current control loops. This algorithm is extremely simple but needs an accurate stator flux estimation to avoid nonzero steady-state errors between the actual and the reference values of torque and flux. Thus, a flux estimator robust to parameter detuning should be used.

The deadbeat control is possible if the voltage commands do not exceed the inverter available voltage. In case of voltage saturation, a proper strategy has to be implemented to allow the best available performance [25].

IV. Torque Saturation Strategy in the Field-Weakening Region

For the machine operation above the rated speed, the machine torque has to be limited due to the dc-link voltage limitation and also due to the inverter current rating. In case of battery fed inverters for electrical vehicles, the dc-link voltage is further limited by the battery discharge. For this reason, a limitation strategy of the DTC reference torque is considered, having as main goal the drive stability and good dynamic performance over the whole speed range of the drive.

The machine model referred to the rotating reference frame (d,q) aligned with the stator flux is

$$\begin{cases} \overline{v}_s^e = R_s \overline{i}_s^e + p\overline{\lambda}_s^e + j\omega_e \overline{\lambda}_s^e \\ 0 = R_r \overline{i}_r^e + p\overline{\lambda}_r^e + j\omega_{\text{slip}} \overline{\lambda}_r^e \\ T_e = 3\frac{P}{2}\lambda_s i_{qs} \end{cases} \quad \begin{cases} \overline{\lambda}_s^e = L_s \overline{i}_s^e + M\overline{i}_r^e \\ \overline{\lambda}_r^e = M\overline{i}_s^e + L_r \overline{i}_r^e \end{cases} \tag{12}$$

where ω_{slip} is the slip frequency.

In steady-state conditions, the (d,q) stator current components can be easily computed from (12) as

$$\begin{cases} i_{ds} = L_s^{-1}\lambda_s + \sigma\tau_r\omega_{\text{slip}} i_{qs} \\ i_{qs} = \frac{1-\sigma}{L_s}\frac{\tau_r}{1+(\sigma\omega_{\text{slip}}\tau_r)^2}\omega_{\text{slip}}\lambda_s \end{cases} \tag{13}$$

where σ is the total leakage factor.

From (12) and (13), the electromagnetic torque is obtained as

$$T_e = 3\frac{P}{2}\frac{1-\sigma}{L_s}\frac{\tau_r}{1+(\sigma\omega_{\text{slip}}\tau_r)^2}\omega_{\text{slip}}\lambda_s^2. \tag{14}$$

The maximum electromagnetic torque value can be computed as a function of the slip frequency by solving

$$\frac{\partial T_e}{\partial \omega_{\text{slip}}} = 0. \tag{15}$$

Thus, the pull-out values of the slip and the electromagnetic torque are [26]

$$T_{e,\text{po}} = 3\frac{P}{2}\frac{1-\sigma}{2\sigma L_s}\lambda_s^2 \quad \omega_{\text{slip,po}} = \frac{1}{\sigma\tau_r}. \tag{16}$$

From (16), it follows that drive stability is achieved only if the slip frequency ω_{slip} is less than the pull-out slip $\omega_{\text{slip,po}}$ or the DTC reference torque T_e^* is limited according to

$$|T_e^*| < T_{e,\text{po}}. \tag{17}$$

The field-weakening strategy of the stator flux reference computation uses the $(1/\omega_r)$ strategy, which is almost optimal for stator flux orientation [26]. Thus, the stator flux reference for the DTC algorithm is generated according to

$$\lambda_s^* = \lambda_{s,\text{rated}}\omega_{\text{base}}|\omega_r|^{-1}, \qquad |\omega_r| > \omega_{\text{base}} \tag{18}$$

where $\lambda_{s,\text{rated}}$ is the rated stator flux and ω_{base} is the drive base speed computed as

$$\omega_{\text{base}} = \frac{V_{s,\max}}{\lambda_{s,\text{rated}}}. \tag{19}$$

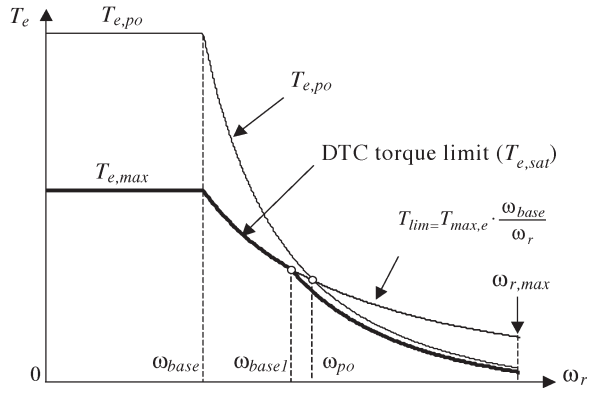

Fig. 10. Torque saturation in the field-weakening range.

In (19), $V_{s,\max}$ is the maximum phase voltage provided by the inverter; it depends on the dc-link voltage, the PWM strategy, and on the inverter switch ON state voltage drops and the inverter dead-time effects.

If $T_{e,\max}$ is the maximum machine overload torque (corresponding to the maximum overload current), then the machine torque must also be limited in field-weakening range to the value given by

$$T_{\lim} = T_{e,\max}\omega_{\text{base}}\left|\omega_r\right|^{-1}. \tag{20}$$

Both (17) and (20) give the ideal DTC maximum value of the reference torque to achieve stable operation of the drive as

$$T_{e,\text{sat}} = \min(T_{\lim}, T_{e,\text{po}}). \tag{21}$$

According to (16)–(21), the DTC reference torque is first limited by the maximum torque curve (20) up to the speed ω_{po}. For speed values higher than ω_{po}, the maximum torque is limited by the pull-out torque curve (16). The boundary speed ω_{po} is computed from (16) and (20) as

$$\omega_{\text{po}} = 3\frac{P}{2}\frac{1-\sigma}{2\sigma L_s}\frac{\lambda_{s,\text{rated}}^2}{T_{\max}}\omega_{\text{base}}. \tag{22}$$

In practice, the field-weakening technique uses a boundary speed ω_{base1}, which is slightly smaller than ω_{po}, as shown in Fig. 10. Up to ω_{base1}, the machine torque is limited by (20); for speeds higher than ω_{base1}, the torque is limited to keep the slip frequency constant and equal to ω_{slip1}, which is the slip frequency corresponding to ω_{base1}. The value of ω_{slip1} can be computed from (16)–(21) as

$$\omega_{\text{slip1}} = \frac{1-\sqrt{1-(2K\sigma)^2}}{2K\sigma^2\tau_r} \tag{23}$$

where $K = T_{\max}L_s(3(P/2)(1-\sigma)(\omega_{\text{base}}/\omega_{\text{base1}})\lambda_{s,\text{rated}}^2)^{-1}$.

The saturation value of the torque for speed values above ω_{base1} will be

$$T_{e,\text{sat}} = 3\frac{P}{2}\frac{1-\sigma}{L_s}\frac{\tau_r}{1+\left(\sigma\omega_{\text{slip1}}\tau_r\right)^2}\omega_{\text{slip1}}\lambda_s^2. \tag{24}$$

In conclusion, the torque saturation strategy in the field-weakening region can be summarized as

$$\begin{cases} T_{e,\text{sat}} = T_{\max}, & \text{if } |\omega_r| \le \omega_{\text{base}} \\ T_{e,\text{sat}} = T_{\max}\omega_{\text{base}}|\omega_r|^{-1}, & \text{if } \omega_{\text{base}} < |\omega_r| \le \omega_{\text{base1}} \\ T_{e,\text{sat}} = 3\frac{P}{2}\frac{1-\sigma}{L_s}\frac{\tau_r\omega_{\text{slip1}}\lambda_s^2}{1+(\sigma\omega_{\text{slip1}}\tau_r)^2}, & \text{if } |\omega_r| > \omega_{\text{base1}}. \end{cases} \tag{25}$$

To prevent problems caused by parameter detuning, the value of ω_{base1} is chosen slightly smaller than ω_{po} to guarantee proper operation of the drive in the deep flux weakening region. That is equivalent to limiting the machine torque to a value slightly smaller than the pull-out torque in order to achieve stable operation for the drive.

V. Experimental Results

The experimental tests have been performed with a 10-kW dual three-phase induction motor prototype whose parameters are given in the Appendix. The switching frequency of the six-phase insulated gate bipolar transistor (IGBT) inverter has been set at 10 kHz. The inverter dc-link voltage is 120 V.

The block diagram of the digital DTC scheme for dual three-phase induction motor drives is shown in Fig. 11.

The control algorithm has been implemented on the dSPACE DS1103 PPC Controller Board. The digital control algorithm uses a 10-kHz sampling frequency. The PWM modulator uses the double zero-sequence injection modulation technique that gives satisfactory results regarding harmonics minimization in the (μ_1, μ_2) subspace [11], [13].

The experimental results are shown in Figs. 12–16 for two different tests. For the first test, a square wave reference speed whose amplitude is equal to 500 r/min to saturate the speed controller is applied to the control system. The transient response of the drive in terms of estimated machine torque T_e, estimated stator flux λ_s, synchronous frame (d, q), stator currents components i_{dqs}, and rotor speed ω_r is shown in Fig. 12.

The results of Fig. 12 show a good flux and torque regulation. The (d, q) synchronous reference frame stator current components are not decoupled, as demonstrated by (13). Thus, any torque transient will affect the d-axis current component, as shown in Fig. 12.

The second test consisted of a startup of the drive to 6000 r/min ($\cong$ 600 Hz) followed by speed reversal using a ramp speed reference. The estimated electromagnetic torque, the stator flux, and the rotor speed for this test are shown in Fig. 13.

The field-weakening strategy described by (18) and (25) computes the reference stator flux and limits the machine torque in order to have a safe and stable operation of the drive up to 600 Hz, as shown by the torque–speed curve depicted in Fig. 14.

The steady-state operation at maximum motor speed ($\cong$ 600 Hz) and no load is illustrated in Fig. 15.

With constant inverter switching frequency operation allowed by the DTC strategy, the machine phase currents are practically sinusoidal, as shown in Figs. 16 and 17 for full-load and no-load operation. However, this advantage is facilitated by the PWM modulator (Fig. 11), which uses the double

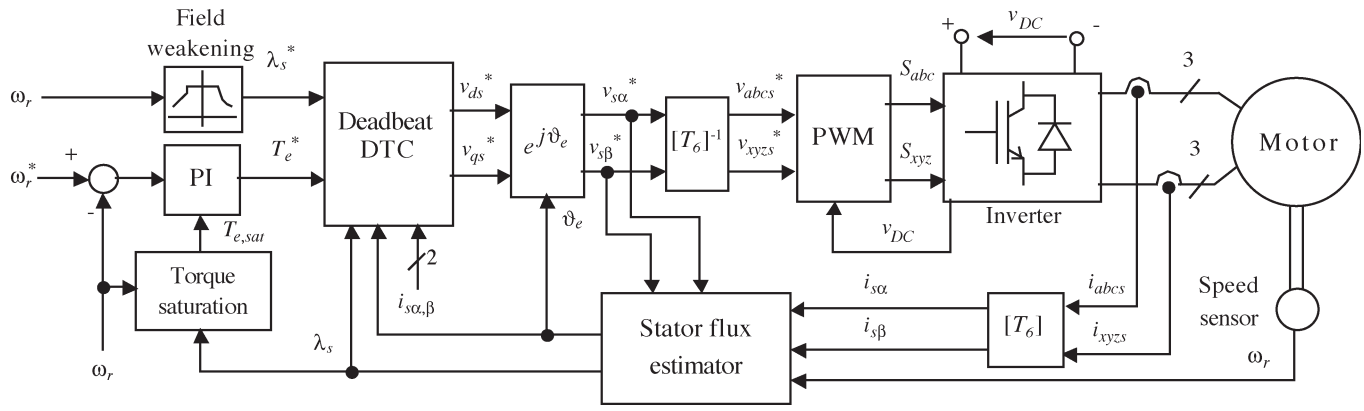

Fig. 11. Experimental dual three-phase induction motor DTC scheme.

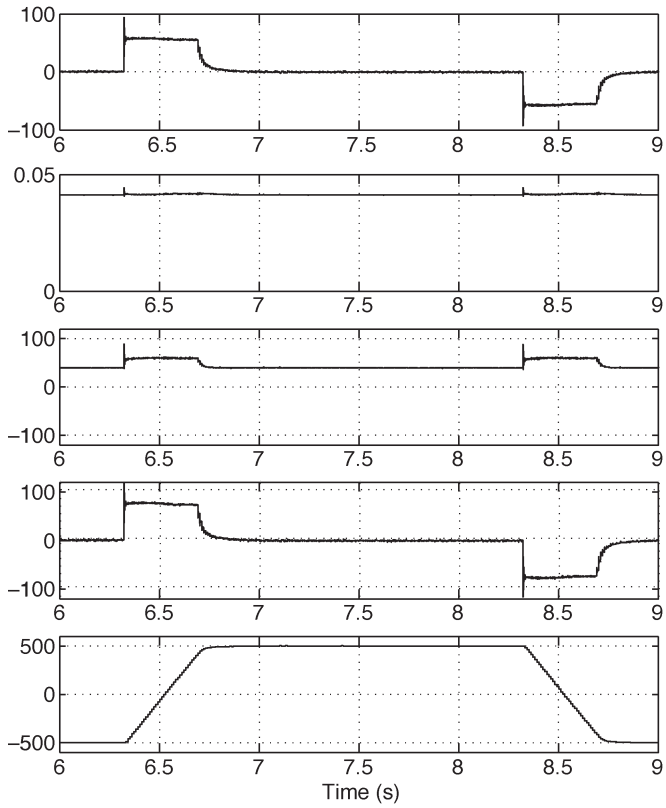

Fig. 12. Experimental results for a square-wave reference speed applied to the drive. From top to bottom: T_e (Nm); λ_s (Vs); i_{ds} (A); i_{qs} (A); and ω_r (r/min).

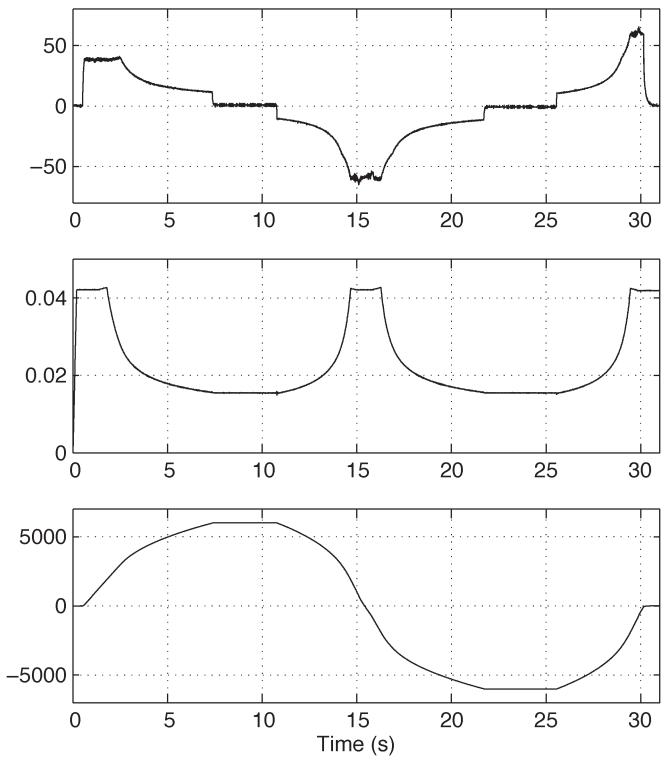

Fig. 13. Startup of the drive with inertial load to 6000 r/min ($\cong$ 600 Hz). From top to bottom: T_e (Nm); λ_s (Vs); and ω_r (r/min).

zero-sequence injection modulation technique. This PWM strategy is able to achieve reasonably low harmonic voltages generated in the (μ_1, μ_2) subspace, reducing in this way the stator loss-producing current harmonics of order $k = 6n \pm 1$ [11], [13].

VI. Conclusion

The paper deals with a direct torque control (DTC) scheme for dual three-phase induction motor drives. The specific aspect of dual three-phase machines is their sensitivity to any harmonic voltage of order $k = 6n \pm 1, (n = 1, 3, 5, \ldots)$ generated in the (μ_1, μ_2) subspace. These harmonic voltages generate large stator loss-producing current harmonics that decrease the drive efficiency.

For this reason, the DTC strategy for dual three-phase drives must have as main goals not only a good stator flux and torque regulation but also a low distortion of the machine phase currents.

Some of the DTC strategies used for the conventional three-phase induction machines have been considered.

- The direct self control (DSC) and switching table-based DTC (ST-DTC) strategies implemented for three-phase machines give a variable switching frequency and distorted machine phase currents, especially at light loads.

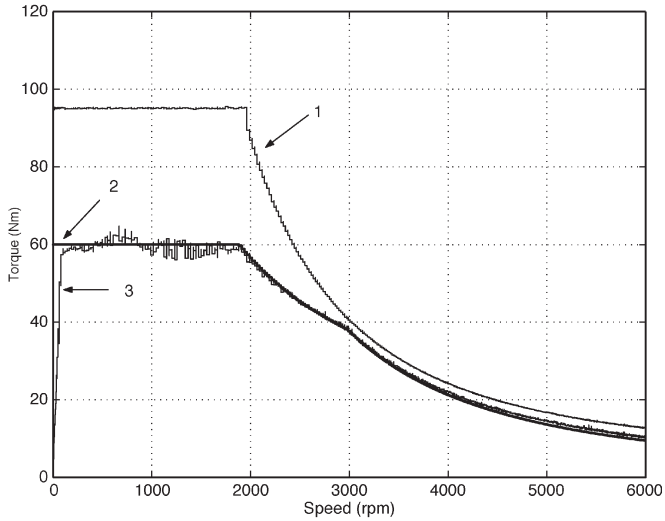

Fig. 14. Torque–speed characteristic under torque saturation conditions. Trace 1: $T_{e,\mathrm{po}}$ (N · m). Trace 2: T_e^* (N · m). Trace 3: T_e (N · m).

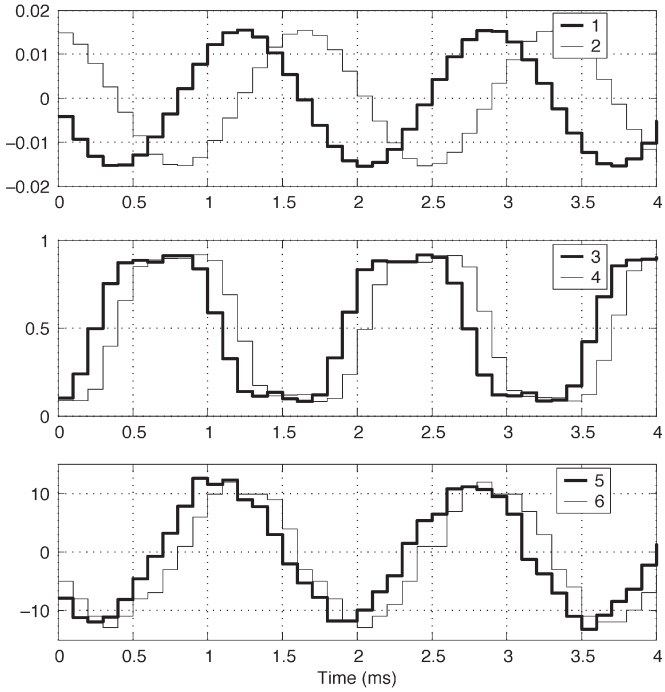

Fig. 15. Steady-state operation at 6000 r/min (≅ 600 Hz) and no load. (1) $\lambda_{s\alpha}$ (Vs); (2) $\lambda_{s\beta}$ (Vs); (3) duty-cycle phase as δ_{as}; (4) duty-cycle phase xs δ_{xs}; (5) $i_{s\alpha}$ (A); (6) $i_{s\beta}$ (A).

- The deadbeat DTC allows, by means of a pulsewidth modulation (PWM) block, constant switching frequency and sinusoidal machine currents; for this reason, this technique has been chosen for the dual three-phase drive presented in this paper. The DTC control scheme has been implemented in the stator flux synchronous reference frame. A reference torque saturation strategy has been used in the field-weakening region to guarantee the drive stability over the whole speed range.

Besides advantages regarding the simplicity of the algorithm, the DTC implementation in synchronous reference frame

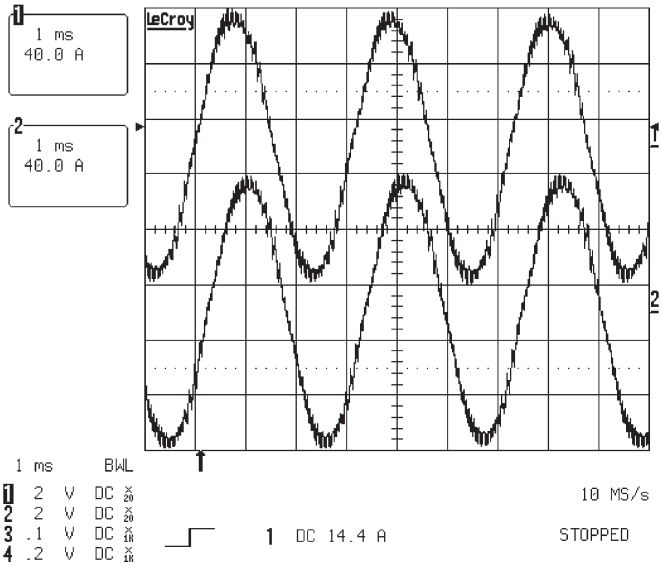

Fig. 16. Machine phase currents during acceleration at full torque. Trace 1: i_{as} (A). Trace 2: i_{xs} (A).

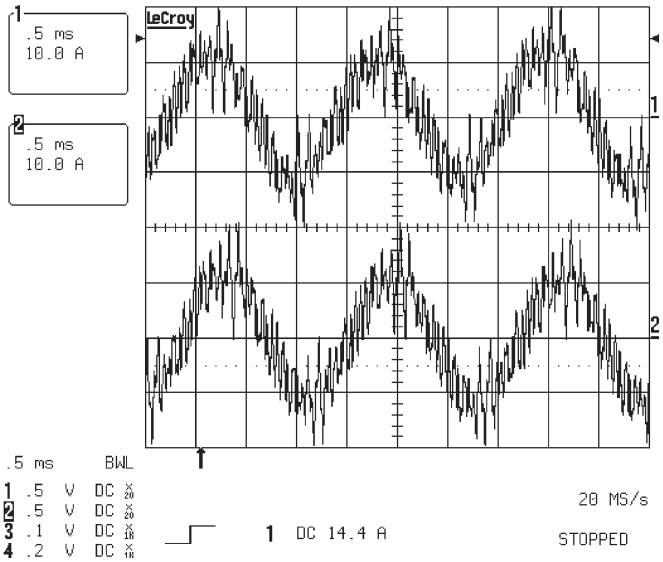

Fig. 17. Machine phase currents at maximum speed (6000 r/min) and no load. Trace 1: i_{as} (A). Trace 2: i_{xs} (A).

avoids computational problems related to the division by zero, which occurs for stationary frame implementation. The additional rotational transformations do not represent an important computational effort for the digital processor.

The experimental results show a good response of the stator flux and the torque in both constant torque and field-weakening regions. For this reason, the discussed DTC scheme could be a possible alternative to FOC schemes for dual three-phase induction motor drives in high-current applications such as electrical vehicles.

APPENDIX

The prototype is a 10-kW 40-V 200-Hz 12-pole full-pitch dual three-phase induction machine with the parameters given in Table I.

TABLE I
MACHINE PARAMETERS

Stator resistance	R_s	0.033 (pu)
Rotor resistance	R_r	0.013 (pu)
Stator leakage inductance	L_{ls}	0.155 (pu)
Rotor leakage inductance	L_{lr}	0.069 (pu)
Magnetizing inductance	M	1.8 (pu)
Inertia	J	0.25 (kgm^2)

The transformation matrix $[T_6]$ is given by

$$[T_6] = \frac{1}{3}\begin{bmatrix} 1 & -\frac{1}{2} & -\frac{1}{2} & \frac{\sqrt{3}}{2} & -\frac{\sqrt{3}}{2} & 0 \\ 0 & \frac{\sqrt{3}}{2} & -\frac{\sqrt{3}}{2} & \frac{1}{2} & \frac{1}{2} & -1 \\ 1 & -\frac{1}{2} & -\frac{1}{2} & -\frac{\sqrt{3}}{2} & \frac{\sqrt{3}}{2} & 0 \\ 0 & -\frac{\sqrt{3}}{2} & \frac{\sqrt{3}}{2} & \frac{1}{2} & \frac{1}{2} & -1 \\ 1 & 1 & 1 & 0 & 0 & 0 \\ 0 & 0 & 0 & 1 & 1 & 1 \end{bmatrix}.$$

REFERENCES

[1] T. M. Jahns, "Improved reliability in solid-state ac drives by means of multiple independent phase-drive units," *IEEE Trans. Ind. Appl.*, vol. IA-16, no. 3, pp. 321–331, May/Jun. 1980.

[2] M. Lazzari and P. Ferraris, "Phase number and their related effects on the characteristics of inverter-fed induction motor drives," in *Conf. Rec. IEEE Industry Applications Society (IAS) Annu. Meeting*, Mexico City, Mexico, Oct. 1983, pp. 494–502.

[3] R. Bojoi, M. Chiadò Caponet, G. Grieco, M. Lazzari, F. Profumo, and A. Tenconi, "Computation and measurements of the dc-link current in six-phase voltage source PWM inverters for ac motor drives," in *Conf. Rec. Power Conversion Conf. (PCC)*, Osaka, Japan, Apr. 2002, pp. 953–958.

[4] G. K. Singh and V. Pant, "Analysis of a multiphase induction machine under fault condition in a phase-redundant AC drive system," *Electr. Mach. Power Syst.*, vol. 28, no. 6, pp. 577–590, Jun. 2000.

[5] R. H. Nelson and P. C. Krause, "Induction machine analysis for arbitrary displacement between multiply winding sets," *IEEE Trans. Power App. Syst.*, vol. PAS-93, no. 3, pp. 841–848, May/Jun. 1974.

[6] Y. Zhao and T. A. Lipo, "Modeling and control of a multi-phase induction machine with structural unbalance," *IEEE Trans. Energy Convers.*, vol. 11, no. 5, pp. 570–577, Sep. 1996.

[7] D. Hadiouche, H. Razik, and A. Rezzoug, "Modeling of a double star induction motor for space vector PWM control," in *Conf. Rec. Int. Conf. Electrical Machines (ICEM)*, Espoo, Finland, 2000, pp. 392–396.

[8] ——, "On the design of dual-stator windings for safe VSI fed AC machine drives," in *Conf. Rec. IEEE Industry Applications Society (IAS) Annu. Meeting*, Chicago, IL, 2001, vol. 3, pp. 1779–1786.

[9] M. A. Abbas, R. Christen, and T. M. Jahns, "Six-phase voltage source inverter driver induction motor," *IEEE Trans. Ind. Appl.*, vol. IA-20, no. 5, pp. 1251–1259, Sep./Oct. 1984.

[10] K. Gopakumar, V. T. Ranganathan, and S. R. Bhat, "Split-phase induction motor operation from PWM voltage source inverter," *IEEE Trans. Ind. Appl.*, vol. 29, no. 5, pp. 927–932, Sep./Oct. 1993.

[11] R. Bojoi, M. Lazzari, F. Profumo, and A. Tenconi, "Digital field oriented control for dual-three phase induction motor drives," *IEEE Trans. Ind. Appl.*, vol. 39, no. 3, pp. 752–760, May/Jun. 2003.

[12] Y. Zhao and T. A. Lipo, "Space vector PWM control of dual three-phase induction machine using vector space decomposition," *IEEE Trans. Ind. Appl.*, vol. 31, no. 5, pp. 1100–1108, Sep./Oct. 1995.

[13] R. Bojoi, A. Tenconi, F. Profumo, G. Griva, and D. Martinello, "Complete analysis and comparative study of digital modulation techniques for dual three-phase AC motor drives," in *Conf. Rec. IEEE Power Electronics Specialists Conf. (PESC)*, Cairns, Australia, 2002, vol. 2, pp. 851–857.

[14] D. Hadiouche, L. Baghli, and A. Rezzoug, "Space vector PWM techniques for dual three-phase AC machine: Analysis, performance evaluation and DSP implementation," in *Conf. Rec. IEEE Industry Applications Society (IAS) Annu. Meeting*, Salt Lake City, UT, 2003, vol. 1, pp. 648–655.

[15] R. Bojoi, A. Tenconi, and F. Profumo, "Digital synchronous frame current regulation for dual-three phase induction motor drives," in *Proc. IEEE Power Electronics Specialists Conf. (PESC)*, Acapulco, Mexico, Jun. 2003, pp. 1475–1480.

[16] P. Vas, *Sensorless Vector and Direct Torque Control*. Oxford, U.K.: Oxford Univ. Press, 1998.

[17] G. Buja, D. Casadei, and G. Serra, "Direct stator flux and torque control of an induction motor: Theoretical analysis and experimental results," in *Conf. Rec. IEEE Industrial Electronics Society Conf. (IECON)*, Aachen, Germany, 1998, vol. 1, pp. T50–T64.

[18] X. Huangsheng, H. A. Toliyat, and L. J. Petersen, "Five-phase induction motor drives with DSP-based control system," *IEEE Trans. Power Electron.*, vol. 17, no. 4, pp. 524–533, Jul. 2002.

[19] M. Depenbrock, "Direct Self-Control (DSC) of inverter-fed induction machine," *IEEE Trans. Power Electron.*, vol. PEL-3, no. 4, pp. 420–429, Oct. 1988.

[20] O. Bruno, A. Landi, and L. Sani, "Harmonic reduction in DSC induction motors with two three-phase stator windings sets," *Electr. Mach. Power Syst.*, vol. 27, no. 12, pp. 1259–1268, Dec. 1999.

[21] K. Hatua and V. Y. Ranganathan, "Direct torque control schemes for split-phase induction machines," in *Conf. Rec. IEEE Industry Applications Society (IAS) Annu. Meeting*, Seattle, WA, 2004, vol. 1, pp. 615–622.

[22] P. Mutschler and E. Flach, "Digital implementation of predictive direct control algorithms for induction motors," in *Conf. Rec. IEEE Industry Applications Society (IAS) Annu. Meeting*, St. Louis, MO, 1998, vol. 1, pp. 444–451.

[23] T. G. Habetler, F. Profumo, M. Pastorelli, and L. M. Tolbert, "Direct torque control of induction machines using space vector modulation," *IEEE Trans. Ind. Appl.*, vol. 28, no. 5, pp. 1045–1053, Sep./Oct. 1992.

[24] G. Griva, F. Profumo, M. Abrate, A. Tenconi, and D. Berruti, "Wide speed range DTC drive performance with new flux weakening control," in *Conf. Rec. IEEE Power Electronics Specialists Conf. (PESC)*, Fukuoka, Japan, 1998, vol. 2, pp. 1599–1604.

[25] G. Griva, T. G. Habetler, F. Profumo, and M. Pastorelli, "Performance evaluation of a direct torque controlled drive in the continuous PWM-square wave transition region," *IEEE Trans. Power Electron.*, vol. 10, no. 4, pp. 464–471, Jul. 1995.

[26] X. Xu, R. de Doncker, and D. W. Novotny, "Stator flux orientation control of induction machines in the field weakening region," in *Conf. Rec. IEEE Industry Applications Society (IAS) Annu. Meeting*, Pittsburgh, PA, 1988, vol. 1, pp. 437–443.

Radu Bojoi received the M.Sc. degree in electrical engineering from the Technical University "Gh. Asachi" Iasi, Iasi, Romania, in 1993 and the Ph.D. degree from the Politecnico di Torino, Turin, Italy, in 2003.

From 1994 to 1999, he was an Assistant Professor in the Department of Electrical Utilization, Electrical Drives and Industrial Automation, Technical University of Iasi. Since 2004, he has been an Assistant Professor at the Department of Electrical Engineering, Politecnico di Torino. His main research fields are DSP- and field-programmable-gate-array (FPGA)-based digital advanced control solutions for three-phase and multiphase electrical drives and power electronic converters.

Francesco Farina received the M.Sc. and Ph.D. degrees in electrical engineering from the Politecnico di Torino, Turin, Italy, in 2001 and 2005, respectively.

He then joined the Department of Electrical Engineering of the Politecnico di Torino, where he is currently a Researcher under grant. His fields of interest are the control design of high-performance multiphase induction motor drives and the sensorless control of brushless motor drives.

Giovanni Griva received the "Laurea" degree in electronic engineering and the Ph.D. degree in electrical engineering from the Politecnico di Torino, Turin, Italy, in 1990 and 1994, respectively.

In 1995, he was an Assistant Professor in the Department of Electrical Engineering, Politecnico di Torino. Since 2002, he has been an Associate Professor. His fields of interest are power electronics conversion, integrated electronic/electromechanical design, high-performance speed servo drives, and applications of power quality issues. He has published over 60 papers in international conference proceedings and technical journals.

Dr. Griva serves as a Reviewer for the Proceedings of the Institution of Electrical Engineers. He was the recipient of the IEEE Industry Applications Society First Prize Paper Award in 1992.

Francesco Profumo (M'88–SM'90) was born in Savona, Italy, in 1953. He graduated with a degree in electrical engineering from the Politecnico di Torino, Turin, Italy, in 1977.

From 1978 to 1984, he was a Senior Engineer for the R&D Ansaldo Group in Genoa, Italy. In 1984, he joined the Department of Electrical Engineering of the Politecnico di Torino, where he was an Associate Professor until 1995. He was a Visiting Professor in the Department of Electrical and Computer Engineering, University of Wisconsin, Madison, from 1986 to 1988, and in the Department of Electrical Engineering and Computer Science, Nagasaki University, Japan, from 1996 to 1997. He is currently a Professor of Electrical Machines and Drives at the Politecnico di Torino and an Adjunct Professor at the University of Bologna. His fields of interest are power electronics conversion, high-power devices, applications of new power devices, integrated electronic/electromechanical design, high-response-speed servo drives, and new electrical machines structures. He has published more than 200 papers in international conference proceedings and technical journals.

Prof. Profumo is an active Member of the IEEE Industry Applications Society (IAS) Drives Committee and serves as Co-Chairman of the same committee (IEEE-IAS Transactions Review Chairman). He was also an AdCom Member of the IEEE Power Electronics Society (PELS). He is a Member of the Technical Program Committees of several International Conferences in the power electronics and motor drives field and was the Technical Co-Chairman of the PCC'02 in Osaka, Japan, in 2002. He has been the Coordinator or Partner of several projects in the frame of the European Commission activities (Tempus, Comett, Joule, Human Capital and Mobility, Alfa, European Union S&T Grant Programme in Japan, Leonardo da Vinci). He won the IEEE-IAS Second Prize Paper Award in 1991 and 1997, and the IEEE-IAS First Prize Paper Award in 1992. He is a Registered Professional Engineer in Italy.

Alberto Tenconi (M'99) received the M.Sc. and Ph.D. degrees in electrical engineering from the Politecnico di Torino, Turin, Italy, in 1986 and 1990, respectively.

From 1988 to 1993, he was with the Electronic System Division of the FIAT Research Center, where he was engaged in the development of electrical vehicle drive systems. He then joined the Department of Electrical Engineering, Politecnico di Torino, where he is now an Associate Professor. His fields of interest are high-performance drives design, new power electronic device applications, and nonconventional electric machines development. The research activity is documented by more than 80 papers published in international journals and conference proceedings. He has participated in many national and European research programs.

Prof. Tenconi is a Reviewer for international journals.